

# Planar magnetic texture on the surface of a topological insulator

Zhaochen Liu,<sup>1</sup> Jing Wang,<sup>1,2,\*</sup> and Congjun Wu<sup>3,4,5,†</sup>

<sup>1</sup>State Key Laboratory of Surface Physics and Department of Physics, Fudan University, Shanghai 200433, China

<sup>2</sup>Institute for Nanoelectronic Devices and Quantum Computing, Fudan University, Shanghai 200433, China

<sup>3</sup>School of Sciences, Westlake University, Hangzhou 310024, Zhejiang, China

<sup>4</sup>Institute for Theoretical Sciences, Westlake University, Hangzhou 310024, Zhejiang, China

<sup>5</sup>Key Laboratory for Quantum Materials of Zhejiang Province, School of Science, Westlake University, Hangzhou 310024, China

We study the planar magnetic textures in an insulating magnetic film coupled to the Dirac surface state of a topological insulator. It is shown that the radial vortex with winding number  $w = \pm 1$  leads to the confinement of Dirac states, where an exact mapping to the Schrödinger equation of a two-dimensional hydrogen atom is found. The fully spin polarized zero energy bound state resembles the zeroth Landau level of Dirac electrons in a uniform out-of-plane magnetic field. Interestingly, when the hybrid system is proximity coupled to an  $s$ -wave superconductor, the existence of Majorana zero modes at Abrikosov vortex depends only on the relative value of the magnetic exchange coupling and the pairing strength. We conclude with a brief discussion on the physical realization with such magnetic textures.

*Introduction.*- Topology has become a central theme in condensed matter physics. Interesting quantum phenomena emerge from the intricate interplay between non-trivial topology and magnetism [1–4]. Two outstanding examples are the quantum anomalous Hall effect and axion insulators discovered in magnetic topological insulators (TI) [5–19]. The exchange coupling between an out-of-plane magnetization and the TI surface state opens a gap in the surface spectrum. The gap opening is accompanied by the emergence of the surface quantum Hall effect with a half-quantized Hall conductance described by the axion electrodynamics [5], which is the physical origin for the topological magnetoelectric effect. It leads to rich phenomena such as the quantum anomalous Hall with a chiral edge state emerging at the magnetic domain wall as well as the topological magneto-optical effect [20–22].

Peculiar physics emerges when the Dirac surface states couple to spatially nonuniform magnetic textures, such as skyrmions and domain walls [4, 23–27]. In this paper, we study theoretically the two-dimensional (2D) magnetic textures, in an insulating ferromagnetic thin film proximity-coupled to TI surface states. The Dirac electron with a radial magnetic vortex with the winding number  $w = \pm 1$  can be exactly mapped to the Schrödinger equation of a 2D hydrogen atom. The fully spin-polarized zero energy bound state resembles the zeroth Landau level of Dirac electrons in a uniform out-of-plane magnetic field. The radial magnetic vortex acts effectively as a magnetic field along  $z$  axis with  $1/r$  dependence. Interestingly, when the system is coupled to an  $s$ -wave superconductor, the existence of emergent Majorana bound states at the Abrikosov vortex core depends only on the relative value of the magnetic exchange coupling and the pairing strength.

*Model.*- The planar magnetic texture we consider exhibits the form of  $\mathbf{S}(\mathbf{r}) \equiv S\mathbf{n}(\mathbf{r}) = S(\cos\vartheta(\mathbf{r}), \sin\vartheta(\mathbf{r}), 0)$ ,

where  $\mathbf{n}(\mathbf{r})$  is the unit vector describing the magnetization direction, and  $\mathbf{r} = (x, y)$ . It is characterized by the topological winding number [28]

$$w = \frac{1}{2\pi} \oint \nabla\vartheta \cdot d\mathbf{r}. \quad (1)$$

Two typical magnetic vortices with  $w = 1$  are illustrated in Fig. 1 (a,b).

In the presence of the magnetic vortex  $\mathbf{n}(\mathbf{r})$ , the surface states of a TI can be described by the Dirac Hamiltonian

$$\mathcal{H} = v_F(\mathbf{k} \times \boldsymbol{\sigma}) \cdot \hat{\mathbf{e}}_z + g_s \mathbf{n}(\mathbf{r}) \cdot \boldsymbol{\sigma}. \quad (2)$$

Here  $\hbar \equiv 1$ ,  $v_F$  is the Fermi velocity,  $\hat{\mathbf{e}}_z$  is the unit vector normal to the surface, and  $\boldsymbol{\sigma} = (\sigma_x, \sigma_y, \sigma_z)$  are the Pauli matrices describing the spin.  $g_s \equiv J' S \rho_s / 2$ ,  $J'$  is the exchange interaction between the local spin and surface electron, and  $\rho_s$  is the sheet density of local spin. Without loss of generality, we set  $g_s/v_F > 0$  and neglect the particle-hole asymmetry.

We notice that the in-plane Zeeman term is equivalent to a vector potential, thus the Hamiltonian becomes

$$\mathcal{H} = v_F [(\mathbf{k} - \mathcal{A}) \times \boldsymbol{\sigma}] \cdot \hat{\mathbf{e}}_z, \quad (3)$$

where  $\mathcal{A}(\mathbf{r}) \equiv (g_s/v_F)(-\sin\vartheta(\mathbf{r}), \cos\vartheta(\mathbf{r}))$ . For a generic  $\mathcal{A}(\mathbf{r})$ , Eq. (3) is difficult to solve analytically. In the following, we assume  $\mathbf{n}(\mathbf{r})$  is rotational invariant along  $z$  axis. The Hamiltonian conserves total angular momentum, and the energy spectrum can be obtained analytically by squaring  $\mathcal{H}$  to solve  $\mathcal{H}^2\psi = E^2\psi$ , which is

$$\mathcal{H}^2/v_F^2 = -\nabla^2 + \mathcal{A}^2 + 2i\mathcal{A} \cdot \nabla + i(\nabla \cdot \mathcal{A}) - \nabla \times \mathcal{A} \cdot \boldsymbol{\sigma}. \quad (4)$$

In terms of the 2D polar coordinates  $(r, \phi)$ , Eq. (4) is separable into the radial and angular parts. Two typical magnetic textures are radial and curling vortices.

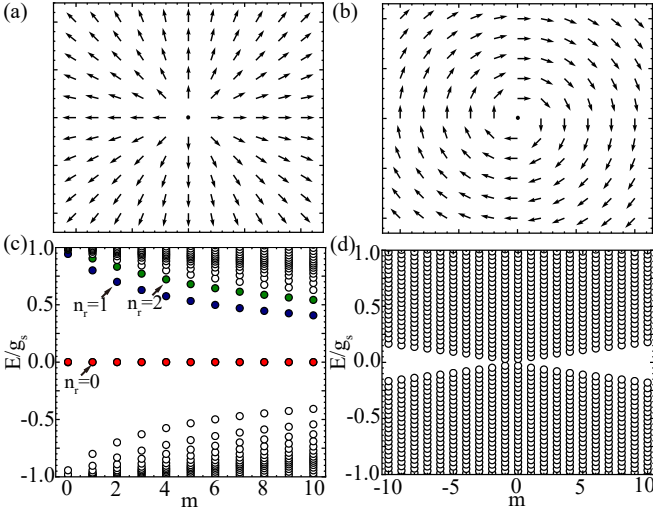


FIG. 1. (a,b) Schematics of the radial and curling planar magnetic vortices in Eq. (5) and Eq.(11), respectively. The vector field represents the direction of local magnetization  $\mathbf{n}(\mathbf{r})$ . (c,d) The numerically calculated energy spectrum for the two cases in (a) and (b) with  $g_s = 2$ ,  $v_F = 10$ , respectively. The bound state spectrum in (c) is bounded by  $|E_{\pm}| < g_s$ .

*Radial vortex.* - First we consider a radial magnetic vortex illustrated in Fig. 1(a),

$$\mathbf{n}_1(\mathbf{r}) = \hat{\mathbf{e}}_r = \frac{1}{r}(x\hat{\mathbf{e}}_x + y\hat{\mathbf{e}}_y), \quad (5)$$

where  $r = \sqrt{x^2 + y^2}$ . Now  $\mathcal{A}_1(\mathbf{r}) \equiv (g_s/v_F)(-y/r, x/r)$ , and  $\nabla \cdot \mathcal{A}_1 = 0$ ,  $\nabla \times \mathcal{A}_1 = (g_s/v_F)(\hat{\mathbf{e}}_z/r)$ ,  $\nabla \cdot \nabla \times \mathcal{A}_1 = 0$ , and  $\mathcal{A}_1 \cdot \nabla = -(g_s/v_F)(y\partial_x - x\partial_y)/r \equiv (g_s/v_F)(iL_z/r)$ , with  $L_z$  the orbital angular momentum operator. Then Eq. (4) becomes

$$\frac{\mathcal{H}_1^2}{v_F^2} = -\frac{1}{r}\partial_r(r\partial_r) + \frac{L_z^2}{r^2} - \frac{g_s}{v_F r}(2L_z + \sigma_z) + \frac{g_s^2}{v_F^2}, \quad (6)$$

where  $\partial_r \equiv \partial/\partial r$ .

Since  $[L_z, \mathcal{H}_1^2] = 0$ , the eigenfunction must have the form as  $\psi(r, \phi) = e^{im\phi}f(r)$ , where the orbital momentum quantum number  $m = 0, \pm 1, \pm 2, \dots$  is connected with the total angular momentum  $j = m + 1/2$ . The radial wave function satisfies the equation

$$\left[ \frac{1}{r}\partial_r(r\partial_r) - \frac{m^2}{r^2} + \frac{g_s}{v_F r}(2m \pm 1) - \frac{g_s^2}{v_F^2} + \frac{E^2}{v_F^2} \right] f(r) = 0. \quad (7)$$

Here  $\pm$  denote  $|\uparrow\rangle$  and  $|\downarrow\rangle$  with  $\sigma_z = +1$  and  $\sigma_z = -1$ , respectively. We define dimensionless quantities

$$r' = r \frac{g_s}{v_F} (m \pm 1/2), \quad E' = \frac{(E/g_s)^2 - 1}{2(m \pm 1/2)^2}. \quad (8)$$

Then Eq. (7) has the exact form as the Schrödinger equation of a 2D hydrogen atom [29], which is the main results

of this paper,

$$\left[ \frac{\partial^2}{\partial r'^2} + \frac{1}{r'} \frac{\partial}{\partial r'} - \frac{m^2}{r'^2} + \left( 2E' + \frac{2}{r'} \right) \right] f(r') = 0. \quad (9)$$

Eq. (9) can be solved algebraically due to the hidden dynamical symmetry of hydrogen atom [30], which is related to the conserved Runge-Lenz operator  $\mathbf{K} \equiv -(i\nabla \times \mathbf{L}_z - \mathbf{L}_z \times i\nabla) - 2\hat{\mathbf{e}}_r$ , satisfying  $[\mathcal{H}^2, \mathbf{K}] = 0$ ,  $[L_z, K_x] = iK_y$ ,  $[L_z, K_y] = -iK_x$  and  $[K_x, K_y] = -4iL_z\mathcal{H}_1^2$ .

Now  $r' > 0$  corresponds to an attractive Coulomb potential, which contains both bound discrete states and unbound continuous states. For  $m \geq 0$ , the eigenvalue of the bound states in Eq. (7) is  $E' = -1/2n_2^2$ , where the principle quantum number  $n_2 \equiv n_r + |m| + 1/2$ , with  $n_r = 0, 1, 2, \dots$ . The radial wave function  $f_{n_r, m}(r') = r'^{|m|} e^{-r'/n_2} F(-n_r, 2|m| + 1, 2r'/n_2)$ , with  $F(\alpha, \gamma; x)$  the confluent hypergeometric function. The degeneracy between  $|\uparrow\rangle$  and  $|\downarrow\rangle$  exists when  $n_{r, \uparrow} = n_{r, \downarrow} + 1$  and  $m_{r, \uparrow} = m_{r, \downarrow} - 1$ , namely  $E_{+, n_r, m} = E_{-, n_r - 1, m + 1}$ . Explicitly, the energy spectrum and (un-normalized) spinor wavefunction of bound states are

$$\begin{aligned} \frac{E_{\pm}}{g_s} &= \pm \left( 1 - \frac{(m + \frac{1}{2})^2}{n_2^2} \right)^{\frac{1}{2}}, \\ \psi_{\pm} &= \begin{pmatrix} e^{im\phi} f_{n_r, m}(r'_+) \\ \mp \frac{\sqrt{(n_r + m + 1)n_r}}{(m + 1)(2m + 1)n_2} e^{i(m + 1)\phi} f_{n_r - 1, m + 1}(r'_-) \end{pmatrix}. \end{aligned} \quad (10)$$

The bound state energies are within the interval between  $\pm g_s$ . The maximum of radial probability density is located at  $r_{\max} \approx n_2^2 a / (m \pm 1/2)$ , with Bohr radius  $a \equiv \hbar v_F / g_s$ . For  $m < 0$  (and  $r' < 0$ ), Eq. (9) corresponds to a repulsive Coulomb potential, there is no bound states and the continuous energy spectrum satisfies  $E' \geq 0$ , namely  $|E| \geq g_s$ .

The branch of states with  $n_r = 0$  are zero energy states and fully spin-polarized as shown in their wave functions  $\psi = (e^{im\phi} f_{0, m}(r'_+), 0)^T$ . They form a flat band resembling the spin polarized zeroth Landau level of Dirac fermions in a uniform magnetic field. However, the magnetic translation symmetry is absent here since  $\nabla \times \mathcal{A}_1$  scales as  $1/r$ . Consequently, the density of states of the zero energy states scales as  $1/r$  as away from the center consistent with the classic radius  $r_m = (m + 1/2)a$ . This situation is similar to the Landau level formation of a 2D Rashba system subject to a harmonic potential [31, 32].

The analytic solutions of energy spectrum is further confirmed by the numerical calculation in Fig. 1(c). Here we choose a disc geometry, and the radial wave function is expanded in terms of the Bessel function [33], the expanding order and disc radius  $\mathcal{R}$  is large enough to ensure convergence and capture the low energy states [34].

*Curling vortex.* - Next we consider a curling magnetic vortex shown in Fig. 1(b)

$$\mathbf{n}_2(\mathbf{r}) = \hat{\mathbf{e}}_{\phi} = \frac{1}{r}(y\hat{\mathbf{e}}_x - x\hat{\mathbf{e}}_y). \quad (11)$$

Then  $\mathcal{A}_2(\mathbf{r}) = (g_s/v_F)(x/r, y/r)$ , with a zero emergent magnetic field  $\nabla \times \mathcal{A}_2 = 0$  and  $\nabla \cdot \mathcal{A}_2 = (g_s/v_F)(1/r)$ . Interestingly, the curling texture can be gauged away, i.e.  $\mathcal{A}_2 \rightarrow \mathcal{A}'_2 + (g/v_F)\nabla r$  and  $\psi \rightarrow \psi' \exp(igr/v_F)$ . There are no bound state but only continuous state solutions [34]. The energy spectrum is numerically calculated in Fig. 1(d).

*Majorana bound state.* It is well known that the localized Majorana zero modes (MZM) arise in the Abrikosov vortex core when the Dirac fermion surface states of a TI is proximity coupled to an  $s$ -wave superconductor [35–40]. Now we study the fate of MZM in the presence of magnetic texture on TI surface.

Now the pairing term  $V = \Delta(\mathbf{r})\psi^\dagger_\uparrow\psi^\dagger_\downarrow + \text{H.c.}$  is added to  $\mathcal{H}$ , where  $\Delta(\mathbf{r})$  is the pairing potential. The system can be diagonalized with the Bogoliubov transformation

$$\psi_\sigma(\mathbf{r}) = \sum_n [u_{n,\sigma}(\mathbf{r})\gamma_n + v_{n,\sigma}^*(\mathbf{r})\gamma_n^\dagger], \quad (12)$$

where  $\gamma_n^\dagger$  create a Bogoliubov quasiparticle. Then the resulting Bogoliubov-de Gennes (BdG) equation is

$$\begin{pmatrix} \mathcal{H} - \mu & \Delta(\mathbf{r}) \\ \Delta^*(\mathbf{r}) & -\sigma_y \mathcal{H}^* \sigma_y + \mu \end{pmatrix} \Phi_n(\mathbf{r}) = E_n \Phi_n(\mathbf{r}), \quad (13)$$

with the BdG energy spectrum  $E_n$  and Nambu wave function  $\Phi_n(\mathbf{r}) = (u_{n\uparrow}(\mathbf{r}), u_{n\downarrow}(\mathbf{r}), v_{n\downarrow}(\mathbf{r}), -v_{n\uparrow}(\mathbf{r}))^T$ .

The BdG equation can be solved numerically for a general pairing potential. Here we study the Abrikosov vortex, where the magnetic flux is contributed by the radial magnetic vortex. Thus the origin of vortex core coincides with the center of magnetic texture as in Fig. 3(a), then Eq. (13) has a cylindrical symmetry. In the polar coordinate, the pairing potential with vortex is  $\Delta(\mathbf{r}) = \Delta_0(r)e^{i\theta} = \Delta_0 \tanh(r/\epsilon_0)e^{i\theta}$ , where  $\epsilon_0$  characterizes the size of vortex core. The wave function can be factorized into

$$\Phi_{n,\ell} = e^{i\ell\theta} (u_{n,\ell\uparrow}, u_{n,\ell+1\downarrow}e^{i\theta}, v_{n,\ell-1\downarrow}e^{-i\theta}, -v_{n,\ell\uparrow})^T,$$

where the principle quantum number  $n$  is determined by solving the radial equation in the basis of Bessel function. The details of numerical calculations are given in Supplemental Material [34]. The calculation is performed on disc of radius  $\mathcal{R} = 40\epsilon_0$ .

Fig. 2 shows the numerical results of BdG energy spectrum for a radial vortex. The MZM is denoted as red dot. As shown in Fig. 2(a,b) for  $\mu = 0$ , the existence of MZM depends only on the relative value of magnetic coupling  $g_s$  and pairing strength  $\Delta_0$ , namely MZM exists for  $g_s < \Delta_0$  and disappears for  $g_s > \Delta_0$ . The zero energy states in Fig. 2(b) are not MZM, but are originated from the zero energy bound states in Fig. 1(c), which deviate from zero by adding a small Zeeman term  $\Delta_z\sigma_z$  into  $\mathcal{H}$ . These results can be simply understood that for  $\mu = 0$ , the chemical potential resides in the bound

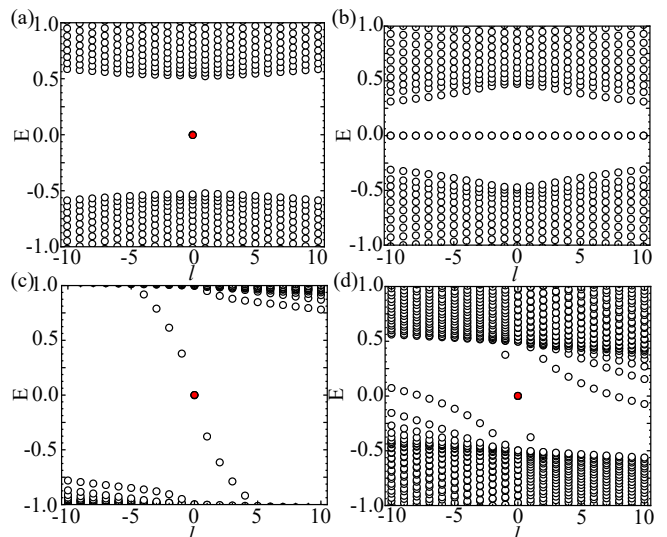


FIG. 2. The BdG energy spectrum of the Abrikosov vortex  $\Delta_0(r)e^{i\theta}$  for radial vortex texture. (a)  $g_s = 0.5$ ,  $\mu = 0$ ,  $\Delta_0 = 1.0$ . (b)  $g_s = 1.0$ ,  $\mu = 0$ ,  $\Delta_0 = 0.5$ . (c)  $g_s = 0.5$ ,  $\mu = 5.0$ ,  $\Delta_0 = 1.0$ . (d)  $g_s = 1.0$ ,  $\mu = 5.0$ ,  $\Delta_0 = 0.5$ . We set  $v_F = 10$ .

state spectrum. Only when the pairing potential exceeds the bound state energy and reaches the continuous state, then MZM from superconducting Dirac fermion proposed by Fu-Kane applies [35]. This is further confirmed in Fig. 2(c,d), where a finite  $\mu > g_s$  crosses the continuous states, MZM always exists in the vortex core. However, for  $\mu > g_s$  case, the system is gapless for finite  $\ell$  when  $g_s > \Delta_0$  shown in Fig. 2(d). We further calculate the vortex case  $\Delta_0(r)e^{i\theta}$  and  $g_s < 0$  [34], where MZM exists  $|g_s| < |\Delta_0|$  and disappears for  $|g_s| > |\Delta_0|$ . The subtle difference between positive and negative  $g_s$  in the vortex case can be seen from the analytic solution. In the limit of  $\epsilon_0 \rightarrow 0$ , the vortex core (where  $\Delta_0$  vanishes) can be taken to have negligible size and the boundary condition at  $r \rightarrow 0$  is unimportant, the analytic zero energy MZM solution is

$$\gamma_{0,+}^\dagger = (1, 0, 0, 1)^T \exp\left(-\int_0^r dr' \frac{\Delta_0(r') + g_s}{v_F}\right). \quad (14)$$

The solution is unphysical at  $r \rightarrow \infty$  when  $g_s < -\Delta_0 < 0$ . For an anti-vortex  $\Delta_0(r)e^{-i\theta}$ , the MZM solution is  $\gamma_{0,-}^\dagger = (0, 1, -1, 0)^T \exp(-\int_0^r dr' (\Delta_0(r') - g_s)/v_F)$ . This represents MZM is from the consistent phase winding between  $\Delta(\mathbf{r})$  and magnetic texture  $\mathcal{A}_1$ .

Now we understand that the radial magnetic texture effectively act like an Abrikosov vortex, where the Abrikosov vortex core is at the center of magnetic texture. We put the Dirac surface state on a sphere, and assume magnetic vortex ( $g_s > 0$ ) and anti-vortex ( $g_s < 0$ ) pairs are located at the north and south poles, respectively. In Fig. 3(a), when the flux line of the effective Abrikosov vortex penetrates the two poles, the pairing

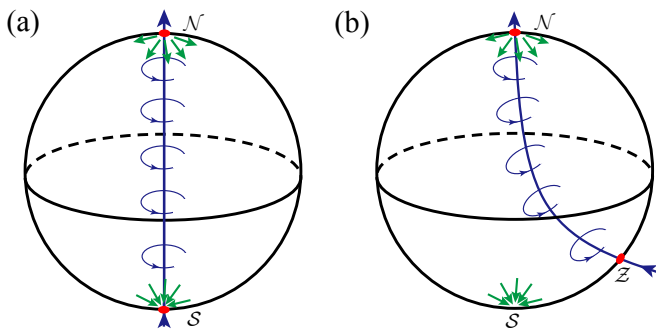


FIG. 3. (a,b) The MZMs are trapped near the surface in the Abrikosov vortex core. The vortex center coincides with the center of magnetic texture in (a) but is shifted away in (b).

potential is  $\Delta_0(r)e^{i\theta}$  and  $\Delta_0(r)e^{-i\theta}$  locally at the north and south poles, respectively. The solutions for MZM at north and south poles are exactly the same, for they are the time-reversal partner of each other. Now in the case of weak exchange interaction  $g_s$ , where the radial magnetic texture could not contribute to a flux quantum. We need add external magnetic field to generate Abrikosov vortex. If the external generated Abrikosov vortex core coincides with the center of the magnetic texture, the MZM locates at the north and south poles. Now the flux line is adiabatically shifted away from the south pole to point  $Z$  in Fig. 3(b). For the condition when the BdG spectrum has a full gap with a vortex-free pairing potential (which is  $g_s < \Delta_0$  illustrated in SM [34]), then the MZM, if exist, can only be localized at the Abrikosov vortex core, since away from the vortex core the surface spectrum is gapped. And the condition for MZM existence in the vortex core at  $Z$  point should be the same as that at north pole ( $g_s < \Delta_0$ ), otherwise it will be contradictory to the fact that MZMs always come into pairs. This argument can also be understood in the limit when  $Z$  point is far away from the origin of magnetic textures, then the magnetization is approximately uniform and parallel to the surface. The parallel in-plane exchange term shift the Dirac point away from  $\Gamma$  point in the perpendicular direction, and introduce pairing-breaking effect between states at  $\mathbf{k}$  and  $-\mathbf{k}$ . The superconducting surface states remains topological with a gap when  $\Delta_0 > g_s$  [41], which is exactly the condition for the existence of MZMs in the vortex core. However, the adiabatical continuity fails when the BdG spectrum is gapless with a vortex-free pairing potential.

*Physical realization.*- The above 2D magnetic texture has a singularity at the origin, while in ferromagnet films with a hard axis pointing along  $z$ -axis, a magnetic vortex with spiralling magnetization configuration could emerge.  $\mathbf{n}(\mathbf{r}) = (\cos \varphi \sqrt{1 - n_z^2}, \sin \varphi \sqrt{1 - n_z^2}, n_z)$ , where  $n_z(r)$  depends only on  $r = \sqrt{x^2 + y^2}$ ,  $\varphi = q\phi + \phi_0$ . The radial vortex  $q = 1, \phi_0 = 0$  is stabilized interfacial Dzyaloshinskii-Moriya interaction (DMI) [42], while

curling vortex  $q = 0, \phi_0 = -\pi/2$  is obtained by minimizing the dipolar interactions [43, 44]. They are the same as that in Fig. 1(a,b) at large  $r$ , respectively. Generally  $n_z(0) = 1$  and decays to  $n_z(\xi_0) = 0$  within the decay length  $\xi_0$ , a typical form is  $n_z(r) = \text{sech}(r/\xi_0)$  with  $\xi_0 \approx 5 \sim 10$  nm. As long as  $a > \xi_0$ , the above study applies to the coupling between Dirac electron and such a realistic magnetic vortex. Here  $a$  is the size of the magnetic vortex within which a flux quantum is obtained. The bound state located at  $r_{\text{max}}$  may be probed by the scanning tunnelling microscopy. For an estimation, take  $v_F \approx 5 \times 10^5$  m/s in  $\text{Bi}_2\text{Te}_3$ , then  $a \approx 30$  nm when  $g_s = 11$  meV.

We propose the artificial two bilayer ferromagnets heterostructure to create magnetic radial vortex, where the dipolar energy is minimized by an antiferromagnetic coupling between them and the radial vortex is obtained by the DMI gradient along the radial direction, namely the DMI parameter monotonically decreases as  $r$  increases.

The incorporation of the magnetic proximity effect into a TI has been exemplified in heterostructures with magnetic insulators [45–47]. Recently a van der Waals magnetic TI  $\text{MnBi}_2\text{Te}_4$  and its descendents have been discovered [48–53], which is compatible with the  $\text{Bi}_2\text{Te}_3$  family materials. Such experimental progress on the material growth and rich material choice of TI and magnetic insulators makes it possible to realize the magnetic vortex in TI heterstructures.

We acknowledge Jiang Xiao for valuable discussions. This work is supported by the National Key Research Program of China under Grant No. 2019YFA0308404, the Natural Science Foundation of China through Grant Nos. 11774065 and 12174066, Science and Technology Commission of Shanghai Municipality under Grant No. 20JC1415900, and the Natural Science Foundation of Shanghai under Grant No. 19ZR1471400. C. W. is supported by the Natural Science Foundation of China through Grant No. 12174317, and No. 11729402.

\* wjingphys@fudan.edu.cn

† wucongjun@westlake.edu.cn

- [1] M. Z. Hasan and C. L. Kane, “*Colloquium*: Topological insulators,” *Rev. Mod. Phys.* **82**, 3045–3067 (2010).
- [2] Xiao-Liang Qi and Shou-Cheng Zhang, “Topological insulators and superconductors,” *Rev. Mod. Phys.* **83**, 1057–1110 (2011).
- [3] Yoshinori Tokura, Kenji Yasuda, and Atsushi Tsukazaki, “Magnetic topological insulators,” *Nat. Rev. Phys.* **1**, 126–143 (2019).
- [4] Wang Yang, Chao Xu, and Congjun Wu, “Single branch of chiral majorana modes from doubly degenerate fermi surfaces,” *Phys. Rev. Research* **2**, 042047 (2020).
- [5] Xiao-Liang Qi, Taylor L. Hughes, and Shou-Cheng Zhang, “Topological field theory of time-reversal invariant insulators,” *Phys. Rev. B* **78**, 195424 (2008).

- [6] Rui Yu, Wei Zhang, Hai-Jun Zhang, Shou-Cheng Zhang, Xi Dai, and Zhong Fang, “Quantized Anomalous Hall Effect in Magnetic Topological Insulators,” *Science* **329**, 61–64 (2010).
- [7] Cui-Zu Chang, Jinsong Zhang, Xiao Feng, Jie Shen, Zuo Cheng Zhang, Minghua Guo, Kang Li, Yunbo Ou, Pang Wei, Li-Li Wang, Zhong-Qing Ji, Yang Feng, Shuaihua Ji, Xi Chen, Jinfeng Jia, Xi Dai, Zhong Fang, Shou-Cheng Zhang, Ke He, Yayu Wang, Li Lu, Xu-Cun Ma, and Qi-Kun Xue, “Experimental Observation of the Quantum Anomalous Hall Effect in a Magnetic Topological Insulator,” *Science* **340**, 167–170 (2013).
- [8] J. G. Checkelsky, R. Yoshimi, A. Tsukazaki, K. S. Takahashi, Y. Kozuka, J. Falson, M. Kawasaki, and Y. Tokura, “Trajectory of the anomalous hall effect towards the quantized state in a ferromagnetic topological insulator,” *Nature Phys.* **10**, 731 (2014).
- [9] Xufeng Kou, Shih-Ting Guo, Yabin Fan, Lei Pan, Murong Lang, Ying Jiang, Qiming Shao, Tianxiao Nie, Koichi Murata, Jianshi Tang, Yong Wang, Liang He, Ting-Kuo Lee, Wei-Li Lee, and Kang L. Wang, “Scale-invariant quantum anomalous hall effect in magnetic topological insulators beyond the two-dimensional limit,” *Phys. Rev. Lett.* **113**, 137201 (2014).
- [10] A. J. Bestwick, E. J. Fox, Xufeng Kou, Lei Pan, Kang L. Wang, and D. Goldhaber-Gordon, “Precise quantization of the anomalous hall effect near zero magnetic field,” *Phys. Rev. Lett.* **114**, 187201 (2015).
- [11] Yujun Deng, Yijun Yu, Meng Zhu Shi, Zhongxun Guo, Zihan Xu, Jing Wang, Xian Hui Chen, and Yuanbo Zhang, “Quantum anomalous hall effect in intrinsic magnetic topological insulator  $\text{mnbi}_2\text{te}_4$ ,” *Science* **367**, 895–900 (2020).
- [12] Jing Wang, Biao Lian, and Shou-Cheng Zhang, “Quantum anomalous hall effect in magnetic topological insulators,” *Phys. Scr.* **T164**, 014003 (2015).
- [13] C.-X. Liu, S.-C. Zhang, and X.-L. Qi, “The quantum anomalous hall effect: Theory and experiment,” *Annu. Rev. Condens. Mat. Phys.* **7**, 301–321 (2016).
- [14] Jing Wang, Biao Lian, Xiao-Liang Qi, and Shou-Cheng Zhang, “Quantized topological magnetoelectric effect of the zero-plateau quantum anomalous Hall state,” *Phys. Rev. B* **92**, 081107 (2015).
- [15] M. Mogi, M. Kawamura, R. Yoshimi, A. Tsukazaki, Y. Kozuka, N. Shirakawa, K. S. Takahashi, M. Kawasaki, and Y. Tokura, “A magnetic heterostructure of topological insulators as a candidate for an axion insulator,” *Nature Mater.* **16**, 516–521 (2017).
- [16] Masataka Mogi, Minoru Kawamura, Atsushi Tsukazaki, Ryutaro Yoshimi, Kei S. Takahashi, Masashi Kawasaki, and Yoshinori Tokura, “Tailoring tricolor structure of magnetic topological insulator for robust axion insulator,” *Sci. Adv.* **3**, eaao1669 (2017).
- [17] S. Grauer, K. M. Fijalkowski, S. Schreyeck, M. Winnerlein, K. Brunner, R. Thomale, C. Gould, and L. W. Molenkamp, “Scaling of the quantum anomalous hall effect as an indicator of axion electrodynamics,” *Phys. Rev. Lett.* **118**, 246801 (2017).
- [18] Di Xiao, Jue Jiang, Jae-Ho Shin, Wenbo Wang, Fei Wang, Yi-Fan Zhao, Chaoxing Liu, Weida Wu, Moses H. W. Chan, Nitin Samarth, and Cui-Zu Chang, “Realization of the Axion Insulator State in Quantum Anomalous Hall Sandwich Heterostructures,” *Phys. Rev. Lett.* **120**, 056801 (2018).
- [19] Chang Liu, Yongchao Wang, Hao Li, Yang Wu, Yaoxin Li, Jiaheng Li, Ke He, Yong Xu, Jinsong Zhang, and Yayu Wang, “Robust axion insulator and chern insulator phases in a two-dimensional antiferromagnetic topological insulator,” *Nature Mat.* **19**, 522–527 (2020).
- [20] Ken N. Okada, Youtarou Takahashi, Masataka Mogi, Ryutaro Yoshimi, Atsushi Tsukazaki, Kei S. Takahashi, Naoki Ogawa, Masashi Kawasaki, and Yoshinori Tokura, “Terahertz spectroscopy on faraday and kerr rotations in a quantum anomalous hall state,” *Nat. Commun.* **7**, 12245 (2016).
- [21] Liang Wu, M. Salehi, N. Koirala, J. Moon, S. Oh, and N. P. Armitage, “Quantized faraday and kerr rotation and axion electrodynamics of a 3d topological insulator,” *Science* **354**, 1124–1127 (2016).
- [22] V. Dziom, A. Shuvaev, A. Pimenov, G. V. Astakhov, C. Ames, K. Bendias, J. Böttcher, G. Tkachov, E. M. Hankiewicz, C. Brüne, H. Buhmann, and L. W. Molenkamp, “Observation of the universal magnetoelectric effect in a 3d topological insulator,” *Nat. Commun.* **8**, 15197 (2017).
- [23] Ion Garate and M. Franz, “Inverse spin-galvanic effect in the interface between a topological insulator and a ferromagnet,” *Phys. Rev. Lett.* **104**, 146802 (2010).
- [24] Kentaro Nomura and Naoto Nagaosa, “Electric charging of magnetic textures on the surface of a topological insulator,” *Phys. Rev. B* **82**, 161401 (2010).
- [25] Takehito Yokoyama, Jiadong Zang, and Naoto Nagaosa, “Theoretical study of the dynamics of magnetization on the topological surface,” *Phys. Rev. B* **81**, 241410 (2010).
- [26] Yaroslav Tserkovnyak and Daniel Loss, “Thin-film magnetization dynamics on the surface of a topological insulator,” *Phys. Rev. Lett.* **108**, 187201 (2012).
- [27] Hilary M. Hurst, Dmitry K. Efimkin, Jiadong Zang, and Victor Galitski, “Charged skyrmions on the surface of a topological insulator,” *Phys. Rev. B* **91**, 060401 (2015).
- [28] D. J. Thouless, *Topological Quantum Numbers in Nonrelativistic Physics* (World Scientific, Singapore, 1998).
- [29] X. L. Yang, S. H. Guo, F. T. Chan, K. W. Wong, and W. Y. Ching, “Analytic solution of a two-dimensional hydrogen atom. i. nonrelativistic theory,” *Phys. Rev. A* **43**, 1186–1196 (1991).
- [30] D. G. W. Parfitt and M. E. Portnoi, “The two-dimensional hydrogen atom revisited,” *J. Math. Phys.* **43**, 4681–4691 (2002).
- [31] Yi Li, Xiangfa Zhou, and Congjun Wu, “Two- and three-dimensional topological insulators with isotropic and parity-breaking landau levels,” *Phys. Rev. B* **85**, 125122 (2012).
- [32] Xiangfa Zhou, Yi Li, Zi Cai, and Congjun Wu, “Unconventional states of bosons with the synthetic spin-orbit coupling,” *J. Phys. B* **46**, 134001 (2013).
- [33] N. Hayashi, T. Isoshima, M. Ichioka, and K. Machida, “Low-lying quasiparticle excitations around a vortex core in quantum limit,” *Phys. Rev. Lett.* **80**, 2921–2924 (1998).
- [34] See Supplemental Material for technical details.
- [35] Liang Fu and C. L. Kane, “Superconducting proximity effect and majorana fermions at the surface of a topological insulator,” *Phys. Rev. Lett.* **100**, 096407 (2008).
- [36] Pavan Hosur, Pouyan Ghaemi, Roger S. K. Mong, and Ashvin Vishwanath, “Majorana modes at the ends of superconductor vortices in doped topological insulators,” *Phys. Rev. Lett.* **107**, 097001 (2011).

- [37] Jin-Peng Xu, Mei-Xiao Wang, Zhi Long Liu, Jian-Feng Ge, Xiaojun Yang, Canhua Liu, Zhu An Xu, Dandan Guan, Chun Lei Gao, Dong Qian, Ying Liu, Qiang-Hua Wang, Fu-Chun Zhang, Qi-Kun Xue, and Jin-Feng Jia, “Experimental detection of a majorana mode in the core of a magnetic vortex inside a topological insulator-superconductor  $\text{Bi}_2\text{Te}_3/\text{NbSe}_2$  heterostructure,” *Phys. Rev. Lett.* **114**, 017001 (2015).
- [38] Gang Xu, Biao Lian, Peizhe Tang, Xiao-Liang Qi, and Shou-Cheng Zhang, “Topological superconductivity on the surface of Fe-based superconductors,” *Phys. Rev. Lett.* **117**, 047001 (2016).
- [39] Dongfei Wang, Lingyuan Kong, Peng Fan, Hui Chen, Shiyu Zhu, Wen Yao Liu, Lu Cao, Yujie Sun, Shixuan Du, John Schneeloch, Ruidan Zhong, Genda Gu, Liang Fu, Hong Ding, and Hong-Jun Gao, “Evidence for majorana bound states in an iron-based superconductor,” *Science* **362**, 333–335 (2018).
- [40] Kun Jiang, Xi Dai, and Ziqiang Wang, “Quantum anomalous vortex and majorana zero mode in iron-based superconductor  $\text{Fe}(\text{Te},\text{Se})$ ,” *Phys. Rev. X* **9**, 011033 (2019).
- [41] Noah F. Q. Yuan and Liang Fu, “Zeeman-induced gapless superconductivity with a partial Fermi surface,” *Phys. Rev. B* **97**, 115139 (2018).
- [42] G. Siracusano, R. Tomasello, A. Giordano, V. Puliafito, B. Azzerboni, O. Ozatay, M. Carpentieri, and G. Finocchio, “Magnetic radial vortex stabilization and efficient manipulation driven by the dzyaloshinskii-moriya interaction and spin-transfer torque,” *Phys. Rev. Lett.* **117**, 087204 (2016).
- [43] T. Shinjo, T. Okuno, R. Hassdorf, K. Shigeto, and T. Ono, “Magnetic vortex core observation in circular dots of permalloy,” *Science* **289**, 930–932 (2000).
- [44] A. Wachowiak, J. Wiebe, M. Bode, O. Pietzsch, M. Morgenstern, and R. Wiesendanger, “Direct observation of internal spin structure of magnetic vortex cores,” *Science* **298**, 577–580 (2002).
- [45] Peng Wei, Ferhat Katmis, Badih A. Assaf, Hadar Steinberg, Pablo Jarillo-Herrero, Donald Heiman, and Jagadeesh S. Moodera, “Exchange-coupling-induced symmetry breaking in topological insulators,” *Phys. Rev. Lett.* **110**, 186807 (2013).
- [46] Ferhat Katmis, Valeria Lauter, Flavio S. Nogueira, Badih A. Assaf, Michelle E. Jamer, Peng Wei, Biswarup Satpati, John W. Freeland, Ilya Eremin, Don Heiman, Pablo Jarillo-Herrero, and Jagadeesh S. Moodera, “A high-temperature ferromagnetic topological insulating phase by proximity coupling,” *Nature* **533**, 513–516 (2016).
- [47] Chi Tang, Cui-Zu Chang, Gejian Zhao, Yawen Liu, Zilong Jiang, Chao-Xing Liu, Martha R. McCartney, David J. Smith, Tingyong Chen, Jagadeesh S. Moodera, and Jing Shi, “Above 400-K robust perpendicular ferromagnetic phase in a topological insulator,” *Sci. Adv.* **3** (2017), 10.1126/sciadv.1700307.
- [48] Dongqin Zhang, Minji Shi, Tongshuai Zhu, Dingyu Xing, Haijun Zhang, and Jing Wang, “Topological axion states in the magnetic insulator  $\text{MnBi}_2\text{Te}_4$  with the quantized magnetoelectric effect,” *Phys. Rev. Lett.* **122**, 206401 (2019).
- [49] Mikhail M. Otrokov, Ilya I. Klimovskikh, Hendrik Bentmann, Alexander Zeugner, Ziya S. Aliev, Sebastian Gass, Anja U. B. Wolter, Alexander V. Koroleva, Dmitry Estyunin, Alexander M. Shikin, María Blanco-Rey, Martin Hoffmann, Alexander Yu. Vyazovskaya, Sergey V. Ereemeev, Yury M. Koroteev, Imamaddin R. Amiraslanov, Mahammad B. Babanly, Nazim T. Mamedov, Nadir A. Abdullayev, Vladimir N. Zverev, Bernd Büchner, Eike F. Schwier, Shiv Kumar, Akio Kimura, Luca Petaccia, Giovanni Di Santo, Raphael C. Vidal, Sonja Schatz, Katharina Köfner, Chul-Hee Min, Simon K. Moser, Thiago R. F. Peixoto, Friedrich Reinert, Arthur Ernst, Pedro M. Echenique, Anna Isaeva, and Evgueni V. Chulkov, “Prediction and observation of an antiferromagnetic topological insulator,” *Nature* **576**, 416–422 (2019).
- [50] Yan Gong, Jingwen Guo, Jiaheng Li, Kejing Zhu, Menghan Liao, Xiaozhi Liu, Qinghua Zhang, Lin Gu, Lin Tang, Xiao Feng, Ding Zhang, Wei Li, Canli Song, Lili Wang, Pu Yu, Xi Chen, Yayu Wang, Hong Yao, Wenhui Duan, Yong Xu, Shou-Cheng Zhang, Xucun Ma, Qi-Kun Xue, and Ke He, “Experimental realization of an intrinsic magnetic topological insulator,” *Chin. Phys. Lett.* **36**, 076801 (2019).
- [51] Jiazhen Wu, Fucui Liu, Masato Sasase, Koichiro Ienaga, Yukiko Obata, Ryu Yukawa, Koji Horiba, Hiroshi Kumigashira, Satoshi Okuma, Takeshi Inoshita, and Hideo Hosono, “Natural van der Waals heterostructural single crystals with both magnetic and topological properties,” *Sci. Adv.* **5** (2019), 10.1126/sciadv.aax9989.
- [52] J.-Q. Yan, Y. H. Liu, D. S. Parker, Y. Wu, A. A. Aczel, M. Matsuda, M. A. McGuire, and B. C. Sales, “A-type antiferromagnetic order in  $\text{MnBi}_4\text{Te}_7$  and  $\text{MnBi}_6\text{Te}_{10}$  single crystals,” *Phys. Rev. Materials* **4**, 054202 (2020).
- [53] Chaowei Hu, Lei Ding, Kyle N. Gordon, Barun Ghosh, Hung-Ju Tien, Haoxiang Li, A. Garrison Linn, Shang-Wei Lien, Cheng-Yi Huang, Scott Mackey, Jinyu Liu, P. V. Sreenivasa Reddy, Bahadur Singh, Amit Agarwal, Arun Bansil, Miao Song, Dongsheng Li, Su-Yang Xu, Hsin Lin, Huibo Cao, Tay-Rong Chang, Dan Dessau, and Ni Ni, “Realization of an intrinsic ferromagnetic topological state in  $\text{MnBi}_8\text{Te}_{13}$ ,” *Sci. Adv.* **6** (2020), 10.1126/sciadv.aba4275.

**SUPPLEMENTARY MATERIAL FOR "PLANAR MAGNETIC TEXTURE ON THE SURFACE OF A TOPOLOGICAL INSULATOR"**

**S1. NUMERICAL METHOD TO DIRAC FERMION COUPLED TO MAGNETIC TEXTURES**

In this section, we provide the detail of numerical calculation method for Dirac fermion with Hamiltonian given by:

$$\begin{aligned} H_0 &= v_F((\mathbf{k} - \mathcal{A}) \times \boldsymbol{\sigma}) \cdot \hat{\mathbf{e}}_z \\ &= v_F(k_x - A_x)\sigma_y - v_F(k_y - A_y)\sigma_x \\ &= \begin{pmatrix} 0 & -v_F(\partial_x - i\partial_y) + v_FA(r, \phi) \\ v_F(\partial_x + i\partial_y) + v_FA^*(r) & 0 \end{pmatrix} \end{aligned} \quad (15)$$

with  $A(r, \phi) = (g_s/v_F)(-iy/r+x/r) = (g_s/v_F)e^{-i\phi}$  for radial vortex and  $A(r, \phi) = (g_s/v_F)(ix/r+y/r) = i(g_s/v_F)e^{-i\phi}$  for curling vortex. We numerically solve this equation in a disk geometry. Cause  $\partial_x \pm i\partial_y = e^{i\pm\phi}(\partial_r \pm i\partial_\phi/r)$ , the wave function can be factorized as

$$\psi_{n,l} = e^{il\phi}(u_{n,l,\uparrow}, u_{n,l+1,\downarrow}e^{i\phi})^T \quad (16)$$

and the radial wave function can be expanded in terms of Bessel function of the first kind

$$u_{n,l} = \sum_{j=1}^N c_{n,j,l} \frac{\sqrt{2}}{R J_{l+1}(\beta_{j,l})} J_l(\beta_{j,l} \frac{r}{R}) \equiv \sum_{j=1}^N c_{n,j,l} \phi_{j,l} \quad (17)$$

where  $J_l$  is m-th order Bessel function of the first kind,  $\beta_{j,l}$  is its j-th zeros, N is cutoff for the expansion and  $R$  is the radius of our disk. Then the Hamiltonian is reduced to  $2N \times 2N$  matrix as

$$H_{BdG} = \begin{pmatrix} 0 & V_{\mu,\mu+1} + A_{\mu,\mu+1} \\ V_{\mu,\mu+1}^T + A_{\mu,\mu+1}^\dagger & 0 \end{pmatrix} \quad (18)$$

with

$$(V_{l,l'})_{i,j} = \frac{2v_F}{R} \frac{\beta_{i,l}\beta_{j,l'}}{\beta_{i,l}^2 - \beta_{j,l'}^2} \quad (A_{l,l'})_{i,j} = \int_0^R r dr A(r) \phi_{i,l} \phi_{j,l'} \quad (19)$$

In the following calculations we choose  $v_F = 10$ ,  $R = 400$ ,  $N = 400$  which is enough to ensure the convergence of the low energy spectrum.

**S2. NUMERICAL METHOD TO DIRAC FERMION BDG HAMILTONIAN**

In presence of pairing vortex  $\Delta(r) = \Delta_0 \tanh(r/\epsilon_0)e^{i\phi}$ , the wave function is given by

$$\Phi_{n,l} = e^{il\phi}(u_{n,l,\uparrow}, u_{n,l+1,\downarrow}e^{i\phi}, v_{n,l-1,\downarrow}e^{-i\phi}, -v_{n,l,\uparrow})^T \quad (20)$$

Following the same method, we expand the radial part by Bessel functions, then the BdG matrix is

$$H_{BdG} = \begin{pmatrix} \Delta_z - \mu & V_{l,l+1} + A_{l,l+1} & \Delta_{l,l-1} & 0 \\ V_{l,l+1}^T + A_{l,l+1}^\dagger & -\Delta_z - \mu & 0 & \Delta_{l+1,l} \\ \Delta_{l,l-1}^T & 0 & \Delta_z + \mu & -V_{l-1,l} + A_{l-1,l} \\ 0 & \Delta_{l+1,l}^T & -V_{l-1,l}^T + A_{l-1,l}^\dagger & -\Delta_z + \mu \end{pmatrix} \quad (21)$$

with  $\mu$  as the Chemical potential and  $\Delta_z$  as the z direction Zeeman field.

As we can see from Fig. 4, the zero mode doesn't split with a nonzero Zeeman field when  $g_s < \Delta_0$ . But zero modes in Fig. 4(b) deviate from zero which indicates they are originated from bound states in Fig. 1(c) of the main text.

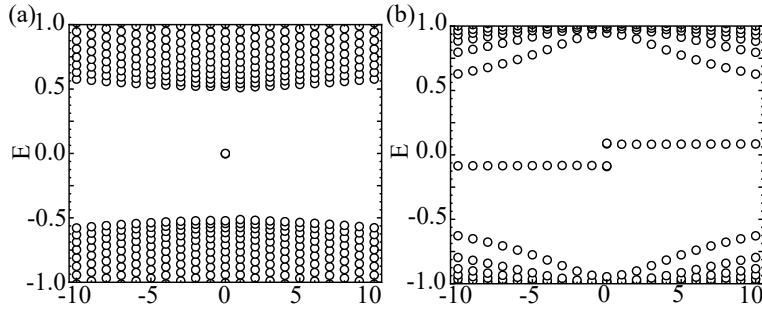


FIG. 4. The BdG spectrum of the Abrikosov vortex  $\Delta_0(r)e^{i\phi}$  in presence of the z-direction Zeeman field for the radial vortex and  $g_s=0.5/2$  for (a,b). Other parameters are  $v_F = 10, \Delta_0 = 1$  and  $\Delta_z = 0.1$ .

Next, let's consider the case with  $g_s < 0$ . The phenomena is similar with  $g_s > 0$  as the majorana zero modes exists only when  $|g_s| > |\Delta_0|$ . And nonzero chemical potential would make the system gapless when  $|g_s| > |\Delta_0|$ .

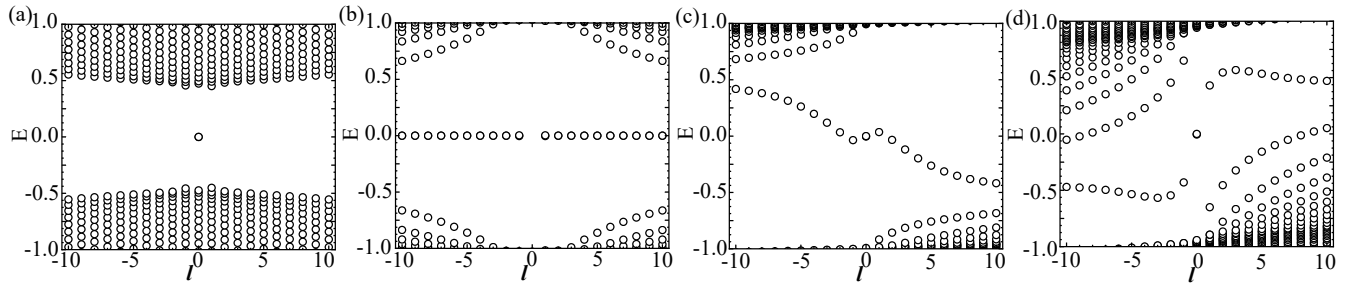


FIG. 5. The BdG spectrum of the Abrikosov vortex  $\Delta_0(r)e^{i\phi}$  with  $g_s < 0$  for the radial vortex. (a)  $g_s = -0.5, \mu = 0$ . (b)  $g_s = -2, \mu = 0$ . (c)  $g_s = -0.5, \mu = 5$ . (d)  $g_s = -1.5, \mu = 5$ . Other parameters are  $v_F = 10, \Delta_0 = 1$ .

### S3. VORTEX FREE BDG SPECTRUM

Finally, we present the BdG spectrum for vortex free superconductor pairing. In this case, the superconductor pairing is  $\Delta(r) = \Delta_0 \tanh(r/\epsilon_0)$ . Due to absence of winding number, the wave should factorized as

$$\Phi_{n,l} = e^{il\phi} (u_{n,l,\uparrow}, u_{n,l+1,\downarrow} e^{i\phi}, v_{n,l,\downarrow} e^{-i\phi}, -v_{n,l+1,\uparrow})^T \quad (22)$$

such that the angular momentum is  $j = l + 1/2$  which implies the absence of the majorana zero mode. Fig. 6 shows the BdG spectrums for radial. Similar to the Abrikosov vortex case, the system is always gapped when  $g_s < \Delta_0$ .

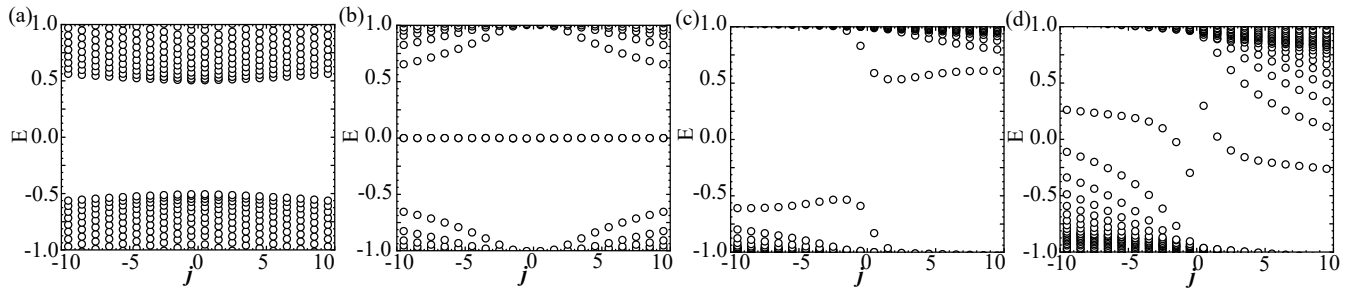


FIG. 6. The BdG spectrum of the Abrikosov vortex  $\Delta_0(r)$  for the radial vortex. (a)  $g_s = 0.5, \mu = 0$ . (b)  $g_s = 2, \mu = 0$ . (c)  $g_s = 0.5, \mu = 5$ . (d)  $g_s = 1.5, \mu = 5$ . Other parameters are  $v_F = 10, \Delta_0 = 1$ .